DISCRIMINATING THE MAIN REPRESENTATIVES OF THE WHITE BLOOD CELL SPECIES ON THE BASIS OF THE FRACTAL PROPERTIES OF THE *DHM* PHASE PROFILE

Eugen I. SCARLAT[1], Mona MIHAILESCU[2], Irina PAUN[3], Mihaela SCARLAT[4]

In order to identify the signatures of the white blood cell (WBC) species, the present study address on discriminating the main WBC representatives based on their fractal properties as revealed by images obtained with digital holographic microscopy (DHM) technique. Since the WBCs are largely varying in contours and volumes, here a multifractal analysis of the phase objects converted in serial data profiles reveals typical properties of three species of WBC namely granulocytes, lymphocytes, and monocytes. The study is performed in terms of the multifractal deviation factor associated to the multifractal spectrum and Lempel-Ziv complexity. The results indicate a promising way to distinguishing the main features of the WBC species complementary to the classical methods based on chromatographic cell imaging.

Keywords: digital holographic microscopy, white blood cells, multifractal deviation factor, Lempel-Ziv complexity.

1. Introduction

The progresses in cell imaging have enabled cost-effective, high-throughput handling and processing of cells and micro-organisms using miniaturized systems at operational fields of view. DHM is providing complementary tools among other techniques like optical coherence tomography [1], or spectrally-resolved phase-shifting interferometry [2] to reveal blood components. Since the phase images are sensitive to both the refractive index and the thickness of the cell, DHM converts both the spatial details and optical inhomogeneity into phase maps whose profiles are further sampled to extract the useful information [3,4]. The spatial resolution in the holographic reconstructions is sufficient to reveal sub-cellular features in order to help the wholeblood analysis [5,6] or more specifically the red blood cell identification [7] and the

[1] Lecturer, Dept. of Physics, University POLITEHNICA of Bucharest,Romania, e-mail egen@physics.pub.ro.
[2] Lecturer, Dept. of Physics, University POLITEHNICA of Bucharest,Romania
[3] Lecturer, Dept. of Physics, University POLITEHNICA of Bucharest,Romania
[4] Oncology Institute *Al. Trestioreanu* Bucharest, Clinical Laboratory

differential red white cell count (leukocyte formulae). Based on the multifractal properties of the scanned phase profile of the WBCs, here two measures to discriminating the most common WBCs are proposed: the multifractal deviation factor (MDF) [8] and the Lempel-Ziv complexity (LZC) [9].

The paper is structured as follows: Section 2 is briefly mentioning the key theoretical elements, and the relevant quantities involved in the study; Section 3 is presenting the experimental setting, Section 4 explains the sampling procedure that converts the image to a time-like data series; in Section 5 are the results and comments; finally, the concluding remarks in Section 6 are reviewing the main findings and original contributions.

2. Theoretical background

The details on experimental hologram recording and reconstruction theory follow [10]. The phase map $\phi(x,y)$ of the optical path d in the wavenumber space or "k space" carries the information about the refractive index n_{ref} intercepted by the object beam along the coordinate z:

$$\phi(x,y) \sim d\left(n_{ref}(x,y,k)\right). \tag{1}$$

Here the phase map roughness of species is investigated in terms of distance to monofractality, i.e. MDF, and LZC. These measures have already been used in other DHM techniques [11,12].

2.1 Multifractal deviation factor

When dealing with the digital versions of phase maps it is possible to create 1-Dim sequences in order to obtain a series $\{s(n)\}_{n=1,N}$ the standard multifractal detrended fluctuation analysis (MF-DFA) can operate [13]. The total number N in the series is greater than 10,000 data points each obtained via a procedure of selecting the phase image shown below. Usually, the width of multifractal spectra can be evaluated in terms of the difference $\Delta\alpha=\alpha_{\max}-\alpha_{\min}$, where $\alpha_{\max}$ and $\alpha_{\min}$ are the extreme values of the Hölder exponents α that characterize the irregularities of the data points in the series [14]:

$$\left|s(n)-P_m(n-n_0)\right| \le C\left|n-n_0\right|^{\alpha} \quad . \tag{2}$$

In Eq.(2) P_m is the polynomial of order m that approximates the series in the current point s_n, and C is a constant. The larger $\Delta\alpha$, the broader the spectrum. Since there are difficulties in computing the extreme values, here the multifractal spectrum is evaluated as the deviation from a monofractal structure [8]:

$$\delta = \alpha_0 - H\,. \tag{3}$$

In Eq.(3) α_0 is the Hölder exponent assigned to the greatest fractal dimension $f(\alpha_0)\leftrightarrow\alpha_0$ of the subsets, while H is the Hurst exponent. Most software packages are directly providing the bell shaped pattern (α, $f(\alpha)$) with the possibility of

finding the coordinates of any point on the curve, including its maximum, so that α_0 could be easily found, while the Hurst exponent is also available in packages using MF-DFA; here the FracLab package was used.

2.2 Lempel-Ziv complexity

To compute LZC, the numerical sequence of data has to first be transformed into a binary sequence. This is achieved by comparing the data with a threshold, usually the median and whenever the signal is larger than or equal to the threshold the particular data is replaced by 1, otherwise by 0. The next step is parsing the obtained symbolic sequence i.e. identifying the number of distinct words present in the sequence. The complexity is given by the number of distinct patterns contained in the sequence. Details on the parsing procedure can be found in [15]. Here the normalized LZC is computed: it gives the complexity of a string relative to that of a genuinely random one. A noise-like experimental series could have LZC index slightly larger than unity because of the finite lengths. Hereafter β is the LZC value denoting the normalized index. The computation is performed using the Chaos Data Analyser software.

3. Experiment

3.1 Blood probes

In order to select the representatives of the leukocytes, the human blood was processed using the standard procedures that reveal the WBCs. Several probes were prepared for chromatographic and holographic identification. Onto grid marked zones, imprinted on microscope slides glass a blood drop is placed and a coverslip over it. That makes possible the identification of *the same* cell for both microscopic imaging: holographic and bright field.

3.2 Optical setting

The experimental configuration is of Mach-Zehnder type interferometer (Fig.1).

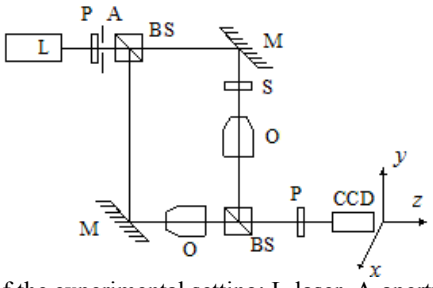

Fig.1. Main elements of the experimental setting: L-laser, A-aperture, BS-beam splitters, M-mirrors, O-microscopes objective, S- sample, P-polarizers, CCD-video camera.

In order to obtain the same curvature of the wave fronts interfering on the CCD sensor, the microscope objectives (O) were identical. The angle between reference and object beams could be trimmed to improve the axial and lateral resolution Δr_l down to 1.4μm while maintaining the depth range $\Delta z \cong 4.9$μm according to the formulae [16]:

$$\Delta r_l = \frac{2\lambda}{\pi A}; \quad \Delta z = \frac{\pi(\Delta r_l)^2}{2\lambda}. \qquad (4)$$

3.3 Phase map

The numerical reconstruction algorithm is based on Fresnel approximation that allows visualization of phase images. A typical image is provided in Fig.2.

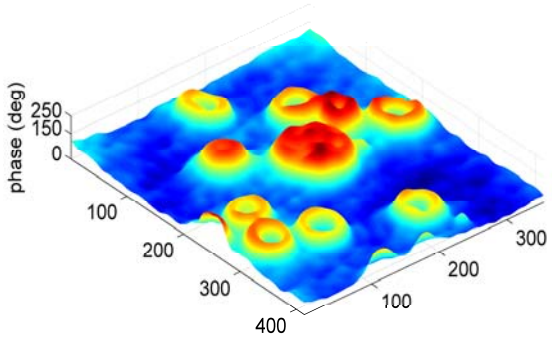

Fig.2. 3D phase maps of the reconstructed blood cells: a WBC surrounded by RBCs

The presence of the nuclei cells as well as the cytoplasm components are turned into phase protuberances that distinguish among the structures of the WBCs.

3.4 Converting the phase maps into data series

The sampling procedure of the phase image of each WBC is designed to grab the maximum number of data points and also to preserve the correlations; consequently the conversion procedure is of phyllotactic type implemented in MatLab according to relations [17]:

$$x_n = c\sqrt{n}\cos(n\varphi); \quad y_n = c\sqrt{n}\sin(n\varphi). \qquad (5)$$

In Eq.(5) n is the index of the element in the series $\{s(n)\}_{n=1,N}$, φ is the step angular growth of approximately 137.5° (golden angle), and c is related to the filling factor.

In order to accommodate the DHM resolution given by Eq.(4) to the spatial dimension of the pixel, matrices as large as 128×128 pixels were used.

Consequently the conversion technique (Fig.3) allows to collecting series of maximum 16,000 points.

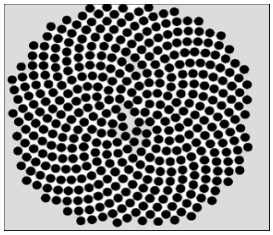

Fig.3. The traces of the sampled pixels over a WBC

4. Results and discussion

4.1 Cell identification

The results are related to the following hypotheses: i/ the identification based on the chromatographic method is assumed to be totally correct – therefore this count will be hereafter labelled as "real count" –, ii/ the refractive indices of the contrast substances are considered to be built-in WBCs, and iii/ the medium which surround the cells is homogeneous.

The "real count" of the investigated WBCs are: 56 granulocytes – out of which the subsequent chromatographic breakdown distinguished 43 neutrophils, 11 eosinophils, and only 2 basophils –, 30 lymphocytes, and 14 monocytes. These numbers are not related to any weight of their presence in the serum. Several results for typical WBCs are given in Fig.4.

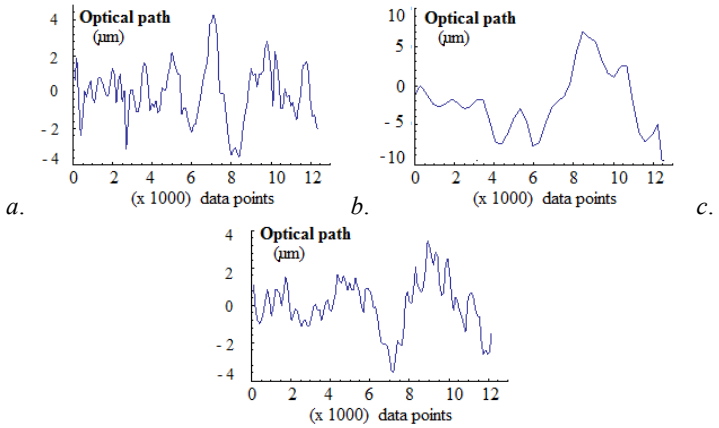

Fig.4. 1-Dim series for granulocyte (*a*), lymphocyte (*b*), and monocyte (*c*).

The results are presented in Table 1, including the standard deviations in the case of each measure and for each species.

Table 1

MFD and LZC for the investigated cells

	Granulocyte	Lymphocyte	Monocyte
MFD δ	0.170 ± 0.097	0.118 ± 0.069	0.086 ± 0.053
LZC β	0.693 ± 0.087	0.562 ± 0.056	0.602 ± 0.020
#	56	30	14

The most "multifractal" appear to be the granulocytes i.e. they have the most complex structure. All species are exhibiting low values for LZC therefore their underlying structures are rather deterministic than uncorrelated and possible random. However, when shuffling the series and destroying the correlations, LZC approaches unity. To the limit of the available number of distinct cells, the standard deviations are approximately half the values of the mean values leading to overlapping of the experimental distributions.

The repeatability with respect to different positions of the starting point of the path in the conversion procedure of the phase image has also been tested. The repeatability has been verified by performing 30 conversions on the same cell chosen at random (Table 2). The standard deviations are small therefore the results are robust against the conversion procedure.

Table 2

The repeatability of MFD and LZC

WBC type	Granulocyte	Lymphocyte	Monocyte
δ (MFD)	0.178 ±0.009	0.125 ± 0.010	0.089 ± 0.007
β (LZC)	0.681 ± 0.002	0.578 ± 0.002	0.592 ± 0.002
#	30	30	30

4.2 False decisions

By denoting q the measure whatever β or δ would be, and assuming Gaussian distributions $G(\mu,\sigma)$, the conversion in standard units ζ is performed for each species (e.g. w_1-granulocyte, w_2-lymphocyte, w_3-monocyte) according to the formula:

$$\zeta_{q,w} = \frac{q - \mu_{q,w}}{\sigma_{q,w}},\ q \in \{\beta,\ \delta\},\ w \in \{w_1,\ w_2,\ w_3\}. \tag{6}$$

For a given cell the probabilities $p(\zeta_{q,w})$ were taken from the table $G(0,1)$ for every species in order to select the largest likelihood and consequently to decide on the group it belongs:

$$p_{q,\max} = \max_{w}\left\{p(\zeta_{q,w})\right\} = p(\zeta_{q,w_j}). \tag{7}$$

The decisions based on Eq.(7) are not fully correlated: for example the monocytes declared as such according to LZC criterion are not fully included in

the set of the monocytes declared as such according to MFD criterion; the case of granulocytes is opposite. Assuming the hypothesis i/, it follows that some decisions are false. The preliminary results are given in Table 3.

Table 3

Decision on WBC type based on separate criteria

WBC species / Measure	Granulocyte	Lymphocyte	Monocyte	False decisions per measure
MFD δ	43 (4 false)	38 (9 false)	19 (8 false)	21 (21%)
LZC β	61 (17 false)	32 (5 false)	7 (1 false)	23 (23%)
"Real count"	56	30	14	

When using the decision of "and" type, i.e. the decision being taken only if the criteria are confirming each other the picture modifies (see Table 4); where not the case of unanimous decision, the cell is "uncertain". This group was missing in the case of the decision on separate criteria, where Eq.(7) forces any cell to belong to one of the WBC species. Now it makes sense to distinguish between false positive (false^{+}) and false negative (false^{-}) decisions.

Table 4

Decision on WBC type based on both criteria

WBC species / Measure	Granulocyte ("real count"=56)	Lymphocyte ("real count"=30)	Monocyte ("real count"=14)
MFD δ **and** LZC β	44 (4 false^{+}, 16 false^{-})	26 (3 false^{+}, 7 false^{-})	5 (0 false^{+}, 9 false^{-})
Uncertain	25 (25%)		

Although the weight of uncertainties is 25%, the decision improved under the reserve of not being fully aware of the medical importance of the cells labelled as "uncertain".

6. Conclusions

Based on DHM principles and on the conversion of the optical path profile into a 1D series as well, the multifractal properties of the WBC phase profile are investigated. Two measures aiming to discriminating the most common WBCs are proposed. The multifractal deviation factor and the Lempel-Ziv complexity are offering promising standing alone or complementary to the classical chromatographic cell imaging. The method is robust against the repeatability of the conversion procedure. The usefulness of the study is to designing a discrimination method with the advantage of processing large amounts of data without contrast agent.

Limiting factors of the present study are at least two: the small number of the cells and the phase shift of the chromatographic substances that are affecting the accuracy of the distributions.

R E F E R E N C E S

[1] *M. Brezinski*, Optical coherence tomography: principles and applications. Academic Press 2006.
[2] *S. Debnath, M. Kothiyal, J. Schmit, and P. Hariharan*, Opt.Express **14**, 4662, 2006.
[3] *T. Anna, D. S. Mehta, and C. Shakher*, ICOP 2009-Int. Conf. on Optics and Photonics, CSIO Chandigarh, India, 2009.
[4] *M. Mihailescu, L. Preda, A. Preda, E. Scarlat*, UPB. Sci. Bull. A, **71**, (2), p. 59-64, 2009.
[5] *P. Marquet et al.,* Opt. Lett. 30 468–470, 2005.
[6] *O. Mudanyali, A. Ozcan, S. Isikman, O. Mudanyali, D. Tseng, and I. Sencan*, SPIE Newsroom, 10.1039/c000453g. 2010.
[7] *M. Mihailescu, J. Costescu*, Optics Express, **20**, (2), 1465-1474, doi.org/10.1364/OE.20.001465, 2012.
[8] *E.I. Scarlat, L. Preda, M. Mihăilescu*, Int. Fed. Autom.Contr. Journ. online, **2** (1) DOI: 10.3182/20090622-3-UK3004.00060: 321-326, 2009.
[9] *A. Lempel*, J. Ziv, IEEE Trans. Inform. Theory, 22, 75-81, 1976.
[10] *J. Kuhn, F. Charriere, T. Colomb, E. Cuche, F. Montfort, Y. Emery, P. Marquet, and C. Depeursinge*, Meas. Sci. Technol. **19**, 074,007–74,008, 2008.
[11] *E.I. Scarlat, M. Mihailescu, A. Sobetkii*, Journ. Optoel. Adv. Mat. **12** (1), 105-109, 2010.
[12] J.*B. Florindo, O.M. Bruno, Chaos*, Solitons and Fractals, **44**, (10), 851-861, doi:10.1016/j.chaos.2011.07.008, 2011.
[13] *J.W. Kantelhardt, S.A. Zschiegner, A. Bunde, S. Havlin, E. Koscielny-Bunde, and H.E. Stanley,* Physica A, **316**, (87), 87-114, 2002.
[14] *D.B. Percival, A.T. Walden*, Cambridge Univ. Press, Cambridge, 2000.
[15] *J. Hu, J. Gao, J.C. Principe*, IEEE Trans. Biomed. Eng. **53** 2606-9, 2006.
[16] *L. Wang L, H. Wu,* B. Masters, Journal of Biomedical Optics, 2008.
[17] *M. Mihailescu*, Optics Express, **18**, (12), 12526-12536, 2010.